

A Two-Scale Approximation for Efficient Representation of Nonlinear Energy Transfers in a Wind Wave Spectrum. Part I: Theoretical Development

DONALD T. RESIO

ERDC-Coastal and Hydraulics Lab, Vicksburg, Mississippi

WILLIAM PERRIE

Fisheries & Oceans Canada, Bedford Institute of Oceanography, Dartmouth, Nova Scotia, Canada

(Manuscript received 11 October 2006, in final form 8 April 2008)

ABSTRACT

A new method for estimating the transfer rates in wind wave spectra is derived and tested, based on a two-scale approximation (TSA) to the total integral for quadruplet wave-wave interactions. Comparisons of this new estimation method to the full integral are given for several idealized spectra, including Joint North Sea Wave Project spectra with different peakednesses, a finite depth case, and cases with perturbations added to underlying parametric spectra. In particular, these comparisons show that the TSA is a significant improvement over the discrete interaction approximation (DIA) in deep water and an even greater improvement in shallow water.

1. Introduction

Hasselmann and Hasselmann (1985) and Hasselmann et al. (1985) argued that, to achieve a proper detailed balance formulation for the physics of wave generation, it was essential to retain the same number of degrees of freedom within all source terms as contained in the modeled directional spectrum. They suggested that models failing to adhere to this criterion would not be able to adapt to complex situations and would require extensive local tuning in applications.

In a detailed-balance wave model, each of the three main source terms believed responsible for wave generation and decay [typically wind input (S_{in}), nonlinear wave-wave interactions (S_{nl}), and wave breaking (S_{ds})] must be cast in a detailed-balance form. Hasselmann et al. (1985) and Komen et al. (1984) noted that S_{in} and S_{ds} could be straightforwardly written in detailed-balance forms. However, no detailed-balance form for S_{nl} existed at that time other than the full Boltzmann integral representation, which even today is considered much too cumbersome for operational wave modeling.

To fill this void, Hasselmann et al. (1985) formulated

the discrete interaction approximation (DIA). This important advance allowed all three primary source terms to be written in a detailed-balance form, leading to a new generation of wave models, termed third-generation (3G) wave models (Komen et al. 1994). Unfortunately, due to practical constraints on computations within operational models, the formulation of the DIA restricted possible four-wave interactions to a subset in which two of the interacting waves are collocated. This subset represents only a small portion of the total interactions included within the general interaction space. Consequently, the DIA is not able to provide a consistent representation for S_{nl} when compared to the full integral solution. Instead, the DIA was calibrated to match the integrated energy transfer rate onto the forward face of the spectrum for a standard Joint North Sea Wave Project (JONSWAP) spectrum (Hasselmann et al. 1973) and, in conjunction with specified forms for wind input and wave breaking, to produce fetch-limited wave growth that compared well with exact computations.

Since the standard JONSWAP spectral form will be utilized in several subsequent comparisons and discussions, it is given here for reference:

$$E(f) = \frac{\alpha g^2}{(2\pi)^4} f^{-5} \exp\left[-1.25\left(\frac{f}{f_p}\right)^4\right] \gamma^\theta, \quad (1)$$

Corresponding author address: William Perrie, Fisheries & Oceans Canada, BIO, Dartmouth, NS BZY4AZ, Canada.
E-mail: perriew@dfo-mpo.gc.ca

where $E(f)$ is the spectral density at f ;

$$\Theta = \exp\left[\frac{-(f - f_p)^2}{2\sigma^2 f_p^2}\right];$$

and

$$\begin{aligned}\sigma &= \sigma_a \quad \text{for } f < f_p, \\ &= \sigma_b \quad \text{for } f \geq f_p.\end{aligned}$$

This spectral characterization has five parameters: the spectral peak frequency (f_p), the equilibrium range coefficient for an f^{-5} -based spectrum (α), peakedness (γ), the spectral width for frequencies less than the spectral peak frequency (σ_a), and the spectral width for frequencies greater than or equal to the spectral peak frequency (σ_b).

Young and Van Vledder (1993) have shown that the nonlinear source term (S_{nl}) is of central importance to the wave generation process; thus, the current state of the art in wave modeling via third-generation models can be significantly impaired by the lack of fidelity in the DIA. Consistent with this expectation, considerable evidence has now accumulated showing that third-generation models do not yield appropriate results for situations when winds blow at oblique angles near a coast or for the case of narrow water bodies (Donelan 1980; Donelan et al. 1985; Pettersson 2004).

The purpose of this paper is to introduce a new concept for approximating nonlinear transfers within wave spectra, the two-scale approximation (TSA). Following a brief treatment of the computational requirements for estimating these nonlinear transfers and an examination of the existing method for approximating nonlinear transfers within present operational models, the TSA concept is developed, starting from an exact integral form for these transfers. Next, the TSA is compared to the “exact” integral for a set of deep water and finite-depth parametric spectra, including several cases for which the DIA does not provide very accurate comparisons to the exact” integral. In the final section, we summarize and present conclusions.

2. Estimation of the nonlinear interaction source term

Hasselmann (1962) and Zakharov and Filonenko (1966) established the theoretical foundation for four-wave interactions within wave spectra. Webb (1978), for the deep water case, and Resio et al. (2001), for finite depth, formulated representative solutions for the transfer integral that have been shown to provide reasonable numerical representations for transfer rates due to these interactions. In general, accurate estimation of S_{nl} for each frequency-direction component

within a spectrum requires the evaluation of $N_k N_\theta N_{loc}$ contributing elements, where N_k is the number of discretized frequency bands in the spectrum, N_θ is the number of discretized angles in the spectrum, and N_{loc} is the number of sample points along the interaction locus (Resio and Perrie 1991). Hence, the number of contributions that must be considered over the entire spectrum will be $O(N_k^2 N_\theta^2 N_{loc})$. A typical operational wave model for open ocean applications uses 20 to 25 frequencies and 24 to 36 angle bands, while coastal models may use 30 to 40 frequencies and 36 angle bands. Resio and Perrie showed that about 30 points along the wave-wave locus of interactions are required to provide an accurate estimate for the full integral. Even with judicious filtering of regions included within the integrand, the number of operations required for a quasi-exact representation of S_{nl} is expected to remain much too large to allow its effective application in practical wave modeling, for some time to come.

At least five different approaches have been made to formulate an accurate, efficient evaluation of the full Boltzmann integral solution for nonlinear transfers in a wave spectrum: 1) parametric representations (Barnett 1968; Ewing 1971; Resio 1981; Hasselmann et al. 1985); 2) local interaction or diffusion operator approximations (Hasselmann et al. 1985; Polnikov 2002; Pushkarev et al. 2004); 3) linear combinations of orthogonal functions (Hasselmann et al. 1985); 4) reduced integration domains (Lin and Perrie 1997, 1999); and 5) the discrete interaction approximation, or DIA (including its variants using multiple sets of quadruplets, termed the MDIA). Benoit (2005) provides a very good review of some of these methods along with some high-precision methods. However, of all these methods, only the DIA has found much success within operational wave models; consequently, this is the only method that will be examined here, in comparison with the TSA.

In Fig. 1, the DIA estimate for S_{nl} , as calibrated by Hasselmann et al. (1985), is compared to the full Boltzmann integral estimate of S_{nl} for a standard JONSWAP spectrum (peakedness parameter, γ , equal to 3.3), with a $\cos^4\theta$ angular distribution of energy around the central wave direction. Although the directionally integrated transfers from the DIA are calibrated to agree with the full integral solution for the forward face of the spectrum, they deviate substantially elsewhere within the spectrum. Figures 2 and 3 provide comparisons of the DIA to the full integral for cases with the peakedness γ equal to 1 and 7. As can be seen here, although the DIA calibration for $\gamma = 3.3$ forces some degree of consistency between results from the DIA and the full integral (at least for the low-frequency lobe of these transfers), this consistency appears to be

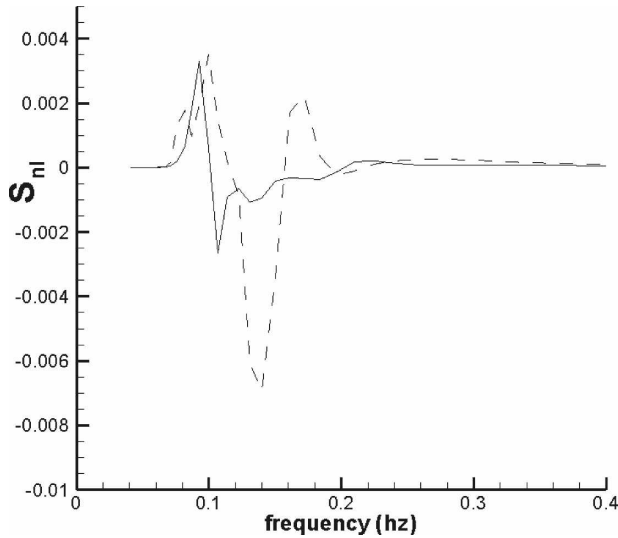


FIG. 1. Comparison of the directionally integrated nonlinear interaction source term, $S_{ni}(f)$, for the DIA (dashed line) with results from the full Boltzmann integral (FBI) (solid line) for a standard JONSWAP spectrum with $\cos^4\theta$ angular distribution of energy around the central wave direction, peak frequency $f_p = 0.1$, and peakedness $\gamma = 3.3$. Units are $m^2 Hz^{-1} s^{-1}$ for S_{ni} .

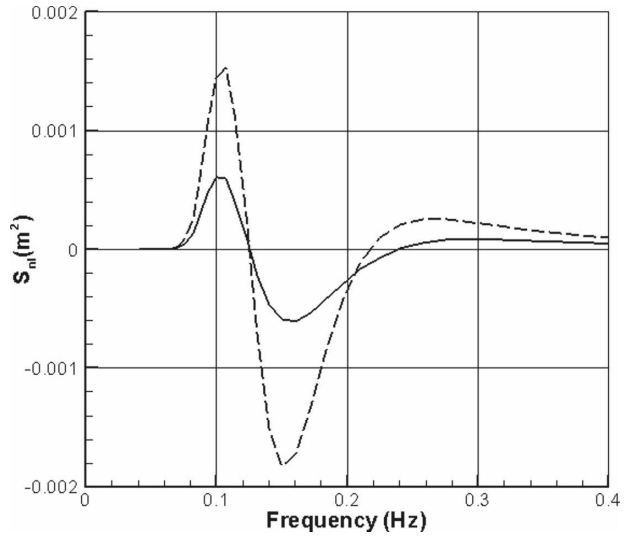


FIG. 2. As in Fig. 1, but for peakedness $\gamma = 1.0$.

limited to a small range of γ values and cannot be construed as representing a general validation for a broad range of spectral shapes.

In particular, as a “fully developed” spectral shape ($\gamma = 1$) is approached, one must apply a large dissipative term near the spectral peak to balance DIA’s substantial overestimation of the nonlinear wave–wave interactions on the forward face of the spectrum to arrest wave growth at this stage. Moreover, the corresponding wind input source term needs to be artificially enhanced on the rear face of the spectrum, for essentially all cases, to compensate for the DIA tendency to overestimate the magnitude of the negative lobe in this spectral region.

The primary reason for the DIA failure to provide suitable estimates for S_{ni} is most likely due to limitations resulting from the DIA integration locus, which falls only along the Phillips (1960) Fig. 8 diagram, whereas the full integral includes contributions from the entire area surrounding any point within a continuous spectrum. This lack of consistency between the integration domains is the primary reason why adding more quadruplets along his Fig. 8 does not produce a very marked improvement in the DIA formulation compared to the total Boltzmann integral.

Given today’s focus on coastal environments, it is important that the operational form for S_{ni} provide accurate estimates not only for deep water spectra but also for spectra in relatively shallow depths. The

method for estimating S_{ni} in modern 3G shallow water was introduced by WAMDI (1988) and has persisted in subsequent wave models such as the SWAN model (Booij et al. 1999). It is based on a scaling argument initially developed by Herterich and Hasselmann (1980). As pointed out by Herterich and Hasselmann, this approach is limited in its applicability to wave spectra for which $k_p h \geq 1$, where k_p is the wavenumber of the spectral peak.

To investigate what happens when the restriction on $k_p h \geq 1$ is violated, let us examine the simple case of a standard JONSWAP spectrum (the calibration case for the DIA) with a peak period of 10 s in a depth of 10.5 m ($k_p h \approx 0.7$). Figure 4 shows a comparison of a scaled

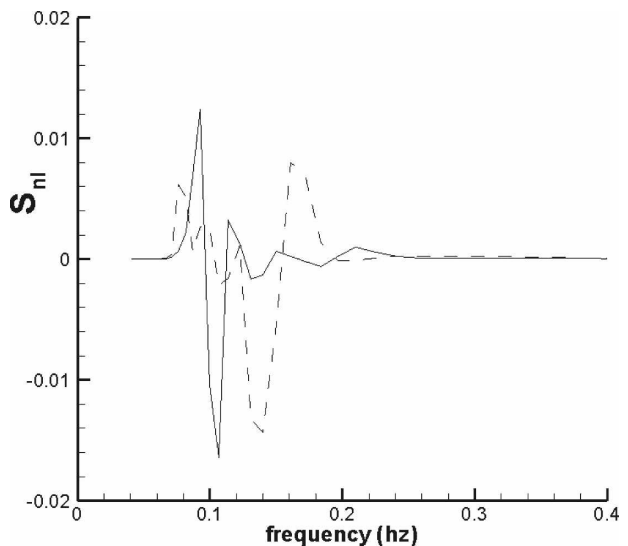


FIG. 3. As in Fig. 1, but for peakedness $\gamma = 7.0$.

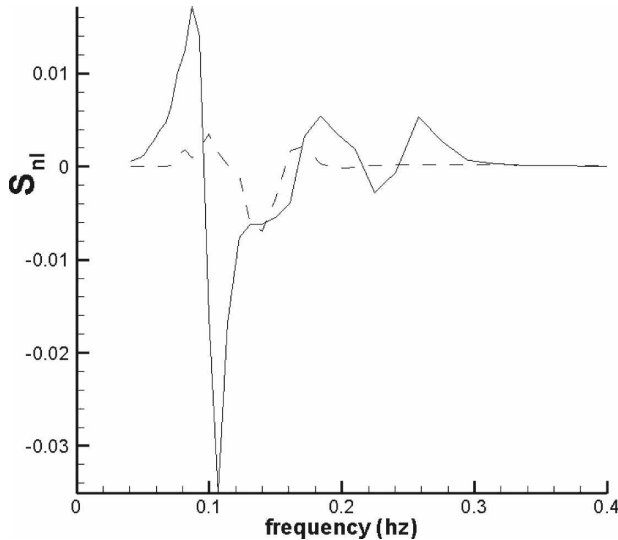


FIG. 4. Comparison of a scaled DIA calculation and an actual full integral, finite depth calculation, showing that the scaled DIA estimate underestimates the positive lobe on the forward face of the spectrum by an order of magnitude for the case of $k_p h = 0.7$ (JONSWAP spectrum with a peak period of 10 s in depth 10.5 m). The dashed line is the Herterich and Hasselmann (1980) scaling of the DIA and the solid line is the finite depth, full integral solution for the same case. Units are $\text{m}^2 \text{Hz}^{-1} \text{s}^{-1}$ for S_{ni} .

DIA calculation and the full-integral, finite-depth calculation for the same spectrum, using the scaling given in Booij et al. (1999). The scaled DIA estimate underestimates the positive lobe on the forward face of the spectrum by about one order of magnitude. It also underestimates the magnitude of the central negative lobe in S_{ni} by a factor of ~ 6 and moves this lobe from the spectral peak region to higher frequencies. Importantly, since the Herterich and Hasselmann (1980) scaling provides only a scalar multiplier for the entire range of frequencies in the spectrum, it does not allow the spectral shape to evolve from its deep water form into the finite-depth form. This evolution, from deep water spectral form to shallow water form, has been well documented by Bouws et al. (1985), who linked changes in spectral form to significant energy losses within coastal wave spectra. This behavior is consistent with the pattern of nonlinear interactions in finite depth as shown by Resio et al. (2001).

3. A two-scale approximation for nonlinear transfers

Hasselmann (1962) showed that the cumulative transfer of energy in a continuous spectrum from one spectral frequency–direction component to another in deep water involves four interacting waves, located at wavenumbers $\mathbf{k}_1, \mathbf{k}_2, \mathbf{k}_3, \mathbf{k}_4$. Following Webb (1978),

the rate of change of action density at a point within a spectrum, \mathbf{k}_1 , can be written as an integral of the transfer rate $T(\mathbf{k}_1, \mathbf{k}_3)$ from wavenumber \mathbf{k}_3 to wavenumber \mathbf{k}_1 :

$$\frac{\partial n(\mathbf{k}_1)}{\partial t} = \iint T(\mathbf{k}_1, \mathbf{k}_3) d\mathbf{k}_3. \quad (2)$$

Webb showed that the transfer rate depends on action densities at all four interacting wavenumbers and that it could be written as

$$T(\mathbf{k}_1, \mathbf{k}_3) = 2 \oint [n_1 n_3 (n_4 - n_2) + n_2 n_4 (n_3 - n_1)] C(\mathbf{k}_1, \mathbf{k}_2, \mathbf{k}_3, \mathbf{k}_4) \theta(|\mathbf{k}_1 - \mathbf{k}_4| - |\mathbf{k}_1 - \mathbf{k}_3|) |\partial W / \partial n|^{-1} ds, \quad (3)$$

where $\theta(x) = 1$, if $x > 0$, and $\theta(x) = 0$, otherwise, and where $\mathbf{k}_4 = \mathbf{k}_1 + \mathbf{k}_2 - \mathbf{k}_3$ and $\mathbf{k}_2 = \mathbf{k}_2(s, \mathbf{k}_1, \mathbf{k}_3)$, and n_i denotes the action density at \mathbf{k}_i . The function W , defined as

$$W = \omega_1 + \omega_2 - \omega_3 - \omega_4, \quad (4)$$

constrains the interactions to ensure energy conservation, s is the locus of points satisfying the condition $W = 0$, and \mathbf{n} is the local orthogonal to the resonant locus. The Webb's (1978) derivation assumed the deep water dispersion relationship

$$\omega_i^2 = gk_i, \quad (5)$$

where $k_i = |\mathbf{k}_i|$. Moreover, Resio et al. (2001) confirmed that Eq. (3) was valid in shallow water, provided the general form of the dispersion relationship was used:

$$\omega_i^2 = gk_i \tanh(k_i h), \quad (6)$$

where h is the water depth, along with the appropriate depth-dependent forms for the coupling coefficient.

The general approach followed here is to decompose a directional spectrum into a parametric (broad-scale) spectrum and a residual (local scale) nonparametric component. The inclusion of the residual component allows this decomposition to retain the same number of degrees of freedom as the modeled spectrum, a prerequisite for 3G model source terms. As will be shown here, this decomposition leads to a representation of the interactions in terms of broad-scale interactions, local-scale interactions, and interactions between the broad-scale and local-scale components of the spectrum. This approach allows the broad-scale interactions and certain portions of the local-scale interactions to be pre-computed.

The accuracy in the TSA has an inherent dependency on the accuracy of the parameterization used in the

representation of the broadscale component of the spectrum. Moreover, if the number of degrees of freedom used to represent the broadscale spectral component were to approach the number of degrees of freedom in the modeled spectrum, the approximation would become quite accurate, even without having to include the effects of the local-scale deviations. However, the estimation of parameter values in an extremely complex spectral parameterization and implementation of a large multidimensional set of pre-computed matrices would likely be almost as time consuming as using the full Boltzmann integral within a wave model. Thus, what we seek here is a small set of parameters that captures sufficient information on the broadscale characteristics of the spectrum (perhaps one to five independent parameters) so that the deviations around this parameterization are as localized as possible. For initial tests with simple idealized spectra, we will show that a simple parameterization based on spectral peakedness and angular spreading achieves this desired goal. Nonlinear energy transfers for the case of simple localized perturbations (even of substantial magnitude) also appear to be quite reasonably represented within the context of such a simple parameterization scheme. It is expected that substantial future effort could be expended toward optimizing the balance between the number of parameters used in the broadscale spectral representation and the magnitude and distribution of deviations left within the local-scale component. However, as will be shown here, even a simple two-parameter representation for the broadscale spectral component significantly outperforms the DIA in terms of accuracy.

We begin by splitting the action density terms, n_i , in Eq. (3) into the sum of two arbitrary components,

$$n_i = \hat{n}_i + n'_i,$$

where the “caret” \hat{n}_i term represents the first component and the “prime” n'_i term represents the second. For this two-component decomposition, the density term in the transfer integral becomes

$$\begin{aligned} N^3 = & \hat{n}_1 \hat{n}_3 (\hat{n}_4 - \hat{n}_2) + \hat{n}_2 \hat{n}_4 (\hat{n}_3 - \hat{n}_1) \\ & + n'_1 n'_3 (n'_4 - n'_2) + n'_2 n'_4 (n'_3 - n'_1) \\ & + \hat{n}_1 \hat{n}_3 (n'_4 - n'_2) + \hat{n}_2 \hat{n}_4 (n'_3 - n'_1) \\ & + n'_1 n'_3 (\hat{n}_4 - \hat{n}_2) + n'_2 n'_4 (\hat{n}_3 - \hat{n}_1) \\ & + \hat{n}_1 n'_3 (\hat{n}_4 - \hat{n}_2) + \hat{n}_2 n'_4 (\hat{n}_3 - \hat{n}_1) \\ & + n'_1 \hat{n}_3 (\hat{n}_4 - \hat{n}_2) + n'_2 \hat{n}_4 (\hat{n}_3 - \hat{n}_1) \\ & + \hat{n}_1 n'_3 (n'_4 - n'_2) + \hat{n}_2 n'_4 (n'_3 - n'_1) \\ & + n'_1 \hat{n}_3 (n'_4 - n'_2) + n'_2 \hat{n}_4 (n'_3 - n'_1). \end{aligned} \quad (7)$$

It can be seen here that the general integral can be written as the sum of interactions among the first component \hat{n}_i terms only (row 1), interactions among the second component n'_i terms only (row 2), and cross-interactions among the two components (rows 3–8). If the two components are of comparable magnitude everywhere, each row in Eq. (7) will also be of comparable magnitude everywhere. In this case, the sum of the cross-interactions will be six times larger than either the interactions involving \hat{n}_i terms alone or the interactions involving n'_i terms alone.

Substituting the form for the spectral density from Eq. (7) into Eq. (3) does not reduce the accuracy of the transfer integral and affords a good means to examine the general problem of bimodal wave spectra, such as might be encountered in a situation with mixed sea and swell. Although this can also be done numerically by subtracting the interactions for a single spectral region from the interactions for the sum of the two spectral regions, the latter approach does not provide the same insight as the use of the “split” density function, where the cross-interaction terms can be examined algebraically. This approach can be used to examine the characteristic transfers from local seas to underlying swell; however, this topic is outside the focus of this paper.

Although the substitution of the two-component spectrum (\hat{n}_i and n'_i) into the cubic density terms in Eq. (3) (the so-called density triplets) provides a convenient methodology for examining interactions between two wave fields, it requires more computational operations than using the simple density form n_i to compute the full integral. Thus, per se, such a partitioning does not provide an effective tool for efficient estimation of nonlinear transfer rates. To accomplish this, we will assume that the distribution of energy within a spectrum can be expressed as the sum of two primary scales (thus the two-scale approximation name): a broadscale variation that can be represented parametrically and a local-scale variation that represents deviations between the parameterized action density levels and the actual action densities within a spectrum.

The TSA attempts to retain the effect of the overall spectral shape on nonlinear transfers via inclusion of the parametric, broadscale interaction term, while allowing the effects of localized deviations and the interactions between the deviations and the large-scale spectral structure to also be included. Inclusion of only the first term \hat{n}_i is comparable to older parametric methods used in representations of S_{nl} (e.g., Barnett 1968; Ewing 1971; Resio 1981). If only the broadscale term was retained, it would reduce the degrees of freedom in the estimation of S_{nl} , which would result in artificial constraints on the behavior of the spectrum. Inclusion of

the second (local) scale n'_i retains the same number of degrees of freedom as the number of discretized spectral elements.

In general, we can write the total interactions for any two-part spectral decomposition of the type introduced here (\hat{n}_i and n'_i) as

$$S_{\text{nl}}(f, \theta) = B + L + X, \quad (8)$$

where B and L represent interactions within the broadscale-only energies \hat{n}_i and the local-scale-only energies n'_i , respectively, and X represents the cross-interactions between the two scales. For the broadscale component, using the exact integral, we can generate a matrix of detailed estimates of S_{nl} for a parametric spectrum defined by a set of n parameters,

$$S_{\text{nl}}(f, \theta)_{\text{broadscale}} = B(f, \theta, x_1, \dots, x_n), \quad (9)$$

where x_i is the value of the i th parameter ($i = 1, n$). From Eq. (9), we see that the number of cases that must be precomputed will depend on both the number of parameters included within the parameterization and the number of discrete increments used to cover the range of relevant parameter values. This point will be addressed in more detail in a subsequent section of this paper. The crux of the remaining problem, in estimating $S_{\text{nl}}(f, \theta)$ via the TSA formulation, is to find a suitable approximation for $L + X$.

The complete transfer integral can be separated into the sum of seven separate integrals, each containing only a single row of Eq. (7) within its density function, plus the broadscale contribution; that is,

$$S_{\text{nl}} = B + \sum_{j=2}^8 \int \int \int \oint N_j^3 C \left| \frac{\partial W}{\partial n} \right|^{-1} ds k_3 d\theta_3 dk_3, \quad (10)$$

where j refers to the j th row in Eq. (7). If all seven terms inside the sum ($j = 2, 8$) were computed, this would represent an approximate eightfold increase in the number of computer operations required, compared to the initial integral form, for an exact representation.

This motivates us to limit the number of terms retained in our functional TSA representation. It will be shown later that there is a substantial computational advantage to neglecting terms involving n'_2 and n'_4 . Consequently, in Eq. (7), all rows and parts of rows containing n'_2 and n'_4 will be neglected in the TSA formulation. Some justification for this can be made based on the fact that local-scale perturbations (n'_i terms) represent deviations around the broadscale basis (\hat{n}_i terms) defined to capture the broadscale variation of energy within the spectrum. Hence, n'_2 and n'_4 , along with their differences and their products, will contain both positive and negative regions as one moves along the respective interaction locus for each. On the other hand,

the broadscale terms \hat{n}_2 and \hat{n}_4 tend to have much longer lengths along the locus s in which the sign is unchanged and therefore should contribute more to the net transfer integral. Since the primary performance metric for the TSA is the ability of the sum of the broad scale and the retained terms to match the full integral, verification of whether our selection of terms is reasonable will be found in comparisons for a range of spectra presented in Part I and Part II (Perrie and Resio 2008, manuscript submitted to *J. Phys. Oceanogr.*). The form of the retained TSA terms also affords the means to examine directly some of the evolutionary characteristics of interacting wave trains. An example of this is given in appendix A.

After eliminating terms containing n'_2 and n'_4 and simplifying, it is possible to write Eq. (10) as

$$\begin{aligned} \frac{\partial n_1}{\partial t} &= B + \int \int \int \oint N_*^3 C \left| \frac{\partial W}{\partial n} \right|^{-1} ds k_3 d\theta_3 dk_3 \\ &= B + (L + X)_*, \end{aligned} \quad (11)$$

where N_*^3 is given by

$$\begin{aligned} N_*^3 &= \hat{n}_2 \hat{n}_4 (n'_3 - n'_1) + n'_1 n'_3 (\hat{n}_4 - \hat{n}_2) + \hat{n}_1 n'_3 (\hat{n}_4 - \hat{n}_2) \\ &\quad + n'_1 \hat{n}_3 (\hat{n}_4 - \hat{n}_2). \end{aligned} \quad (12)$$

The subscript asterisk, after the parenthesis in Eq. (11), indicates that the L and X scale interaction terms include only the density terms given in Eq. (12).

As both \hat{n}_2 and \hat{n}_4 depend only on the same broadscale set of parameters (x_1, \dots, x_n), these can be used as the basis for computing all line integral quantities involving \hat{n}_2 and \hat{n}_4 in Eq. (11). It can be seen from Eq. (12) that this representation retains all broadscale terms in the density equation and is therefore an exact solution for the parametric portion of the spectrum. The local-scale and cross-scale interactions retain only the set of densities that neglect contributions due to n'_2 and n'_4 .

Webb (1978) introduced the concept of “diffusive” and “pumped” transfers of energy, with the diffusive transfers from k_3 to k_1 involving the difference between the action densities at k_3 and k_1 and the pumped transfers involving the product of the densities at k_3 and k_1 . It should be noted that the contributions to the total integral around the locus can be simplified to a constant depending only on the broadscale densities times a multiplicative or difference function of the local-scale densities; that is,

$$\begin{aligned} T_p(k_1, k_3) &= \oint (n'_1 n'_3) C \left| \frac{\partial W}{\partial n} \right|^{-1} (\hat{n}_4 - \hat{n}_2) ds = \Lambda_p (n'_1 n'_3) \\ T_d(k_1, k_3) &= \oint (n'_3 - n'_1) C \left| \frac{\partial W}{\partial n} \right|^{-1} \hat{n}_2 \hat{n}_4 ds = \Lambda_d (n'_3 - n'_1), \end{aligned}$$

where Λ_p and Λ_d are constants that depend only on the broadscale densities (with subscripts p and d denoting their role in pumped and diffusive transfers, respectively). This is an exact relationship for this substitution since only n_2 and n_4 vary around the locus.

The structure of the interaction integral is such that any linear scaling coefficient used in the formulation of

a spectrum will appear as a cubic term in the estimated transfer rates, independent of the shape of the spectrum (i.e., whether it has f^{-4} or f^{-5} or any other basis for its shape). Therefore, making use of wavenumber, linear scaling coefficient, and angle scaling relations we can write Eq. (12) as

$$\begin{aligned} \frac{\partial n_1}{\partial t} = & \left(\frac{k}{k_0}\right)^{-19/2} \left\{ B \left[\left(\frac{s}{s_0}\right) \left(\frac{k}{k_0}\right)^p \right]^3 \right. \\ & + \left. \left[\left(\frac{s}{s_0}\right) \left(\frac{k}{k_0}\right)^p \right]^2 \int \int (\hat{n}_1 n'_3 + n'_1 \hat{n}_3 + n'_1 n'_3) \Lambda_p(\hat{n}_2 - \hat{n}_4, \mathbf{k}_1, k_*, \theta_*, x_1, \dots, x_n) k_* d\theta_* dk_* \right. \right. \\ & \left. \left. + \left[\left(\frac{s}{s_0}\right) \left(\frac{k}{k_0}\right)^p \right]^2 \int \int (n'_1 - n'_3) \Lambda_d(\hat{n}_2 \hat{n}_4, \mathbf{k}_1, k_*, \theta_*, x_1, \dots, x_n) k_* d\theta_* dk_* \right] \right\}, \end{aligned} \tag{13}$$

where

$$\begin{aligned} \Lambda_p(\hat{n}_2 - \hat{n}_4, \mathbf{k}_1, k_*, \theta_*, x_1, \dots, x_n) &= \oint C \left| \frac{\partial W}{\partial n} \right|^{-1} (\hat{n}_4 - \hat{n}_2) ds, \\ \Lambda_d(\hat{n}_2 \hat{n}_4, \mathbf{k}_1, k_*, \theta_*, x_1, \dots, x_n) &= \oint C \left| \frac{\partial W}{\partial n} \right|^{-1} \hat{n}_2 \hat{n}_4 ds, \end{aligned}$$

with the notation for the pumping and diffusion constants expanded to show their dependence on the parameter set used to define the broadscale (parametric) component of the spectrum; p is the power law for the (dimensionally consistent) spectral parameterization being applied, which is typically either f^{-4} or f^{-5} but not restricted to these values. Here (s/s_0) is the ratio of the actual linear scaling coefficient to a reference linear scaling coefficient (essentially the ratio of the spectral steepness parameters) for the broadscale spectral component, and (k/k_0) is the ratio of wavenumbers in the reference spectrum to the associated wavenumbers in the spectrum being integrated to the wavenumber of the spectral peak of the reference spectrum). In this equation, θ_* and k_* are defined as

$$\theta_* = \theta_3 - \theta_1 \tag{14}$$

and

$$k_* = \left(\frac{k_3 - k_1}{k_p} \right). \tag{15}$$

For the f^{-5} -based JONSWAP spectrum, s would be equivalent to the Phillips α coefficient in Eq. (1); for an f^{-4} -based spectrum, typically defined as $E(f) \approx \beta f^{-4}$, s

would be equivalent to β ; and, in general, it could be any linear multiplicative term used to scale a spectrum. The power of s can be seen to equal the number of scaled (broad scale) densities in each of the integrals used in the reference matrices (Λ_d and Λ_p) defined above. The scaling factor for wavenumber similarly comes from the total wavenumber dimensions included in the coupling coefficient ($\sim k^6$), the Jacobian term ($\sim k^{1/2}$), and the phase space terms ($ds k dk \sim k^3$).

An important computational advantage of Eq. (13) is that, even though both local-scale and cross-interaction contributions to the transfer integral are retained for the set of terms included within the TSA, all terms involving the line integral along s can be precomputed within the same discretized computational basis used to estimate B . Integration around these loci constitutes the innermost loop for computations within the exact integration method. Numerical experiments with the Webb–Resio–Tracy (WRT) method (Tracy and Resio 1982) [for details of this method see Van Vledder (2006)] show that this innermost loop represents between 99.5% and 99.7% of the total computation time in these calculations. Retaining the same integration domain as the complete integral can therefore reduce the time required for computations by about a factor of 250 to 500. Additional reductions in TSA run time can be achieved by 1) limiting the number of points at which S_{nl} is evaluated and 2) limiting the integration domain via restrictions on k_* and θ_* .

Similar to the WRT integration method (on which this approximation is based), the TSA method conserves action, energy, and momentum within the limits of the numerical approximation and spectral discretization used. As it is based on a transfer integral form for

the Boltzmann equation $[T(\mathbf{k}_1, \mathbf{k}_3)]$, each transfer of energy into \mathbf{k}_1 from \mathbf{k}_3 accounts for a matching loss of energy at \mathbf{k}_3 within this approximation. The delta functions for \mathbf{k} and ω ensure that momentum and action, respectively, are also conserved. It should be noted that as the DIA is also conservative, this is not a relative advantage for the new TSA method.

4. Tests of the TSA for parametric spectra

A number of tests are required to establish the viability of the TSA formulation for spectral wave modeling. Following the approach of the initial paper on the DIA by Hasselmann et al. (1985), tests here will be limited to static (i.e., not time stepping) comparisons between the TSA and the full-integral solution, for nonlinear transfers in deep water. As noted previously and as can be seen from the structure of Eq. (13), it is apparent that the accuracy of the parameterization used for B will directly influence the accuracy of this approximation. Because the purpose of this paper is to introduce the two-scale approximation and to demonstrate its relevance for wave modeling, we shall begin with a simple (one parameter) parameterization here. There will, of course, be a significant trade-off between increasing the number of parameters used for the broadscale (parametric) component of the spectrum and the number of calculations required to populate the matrices for B , Λ_p , and Λ_d in Eq. (13). The number of dimensions used in the broadscale parameterization will also influence the time required for any interpolation between discrete points, unless the number of categories within the categorizations are sufficiently small that no interpolation is required. For reference, the number of increments of rings and angles used in all TSA integrations shown here is ± 6 rings and ± 6 angles around each point where S_{nl} is evaluated.

In a system of equations that incorporates parametric elements, it is advantageous to ensure that the basis for the parametric solution is one that represents a long-term equilibrium solution for that system of equations. For wind wave spectra, it has been clearly demonstrated that the long-term evolution of spectra will tend to force a spectrum to an f^{-4} form in deep water (Zakharov and Filonenko 1966) and more generally to a $k^{-5/2}$ form in finite depth water (Resio et al. 2001). As such, we will not use the conventional JONSWAP parameterization (which has an f^{-5} form) here. Rather, we use a $k^{-5/2}$ (or equivalently f^{-4} form in deep water) instead for our parameterization.

Motivated by the JONSWAP formulation, let us assume that a simple characterization of the broadscale structure of deep water wave spectra can be accom-

plished by five parameters, f_p , β , κ , σ_a , and σ_b , where these are respectively defined as the spectral peak frequency, the equilibrium range coefficient for an f^{-4} -based spectrum, a spectral peakedness parameter (as described in Long and Resio 2007), a spectral width parameter for the forward face of the spectrum (low-frequency side of the spectral peak), and a spectral width parameter for the rear face of the spectrum (high-frequency side of the spectral peak). It is possible to show, both analytically and numerically, that wave-wave interactions for two f^{-4} -based spectra, as defined here, with the same values for κ , σ_a , and σ_b along with the same directional distributions of energy, are exactly related by

$$S'_{\text{nl}}(\lambda^{-1}f, \theta) = \left(\frac{\beta'}{\beta}\right)^3 \left(\frac{f'_p}{f_p}\right)^{-1} S_{\text{nl}}(f, \theta), \quad (16)$$

where the prime is used to denote the values of β and f_p for a second spectrum and $\lambda = f_p/f'$. Thus, β and f_p can both be algebraically factored out of this type of parametric representation for a spectrum while still retaining exact information for the nonlinear transfer rates. This scaling is consistent with the wavenumber scaling used in Eq. (13). If we further simplify the parameterization by fixing both spectral width parameters to specific values, the peakedness parameter κ is left as the only free parameter in the spectral representation (at least along the frequency axis). For simplicity, we shall begin by assuming the same directional distribution ($\cos^4\theta$) as used in the DIA tests shown in Figs. 1–4. For all tests shown here, all precomputed terms are retrieved from matrices of the form $\mathbf{B}(f, \theta, \kappa)$, $\Lambda_p(f, \theta, \kappa)$, and $\Lambda_d(f, \theta, \kappa)$, with κ discretized in increments of 0.1 over a range extending from 0.4 to 4 and with f and θ collocated with the discrete frequencies and angles, respectively, at which the exact integration is computed.

As the JONSWAP spectrum is an f^{-5} -based spectrum rather than an f^{-4} -based spectrum, tests with this spectral form should provide a good comparison for the TSA, since deviations from the parametric shape (the local-scale spectral component) will be relatively broadly distributed. Thus, the broadband spectrum has an f^{-4} tail whereas the test spectrum has an f^{-5} tail. Figures 5, 6, and 7 provide comparisons of the directionally integrated TSA results to the full-integral solution for JONSWAP spectra with peakednesses equal to 1, 3.3, and 7. The contribution to the TSA from the parametric solution alone is also shown in these figures. Overall, as these are relatively simple spectra, the basic parametric representation (the interactions among only the B -scale spectral components) provides a reasonable

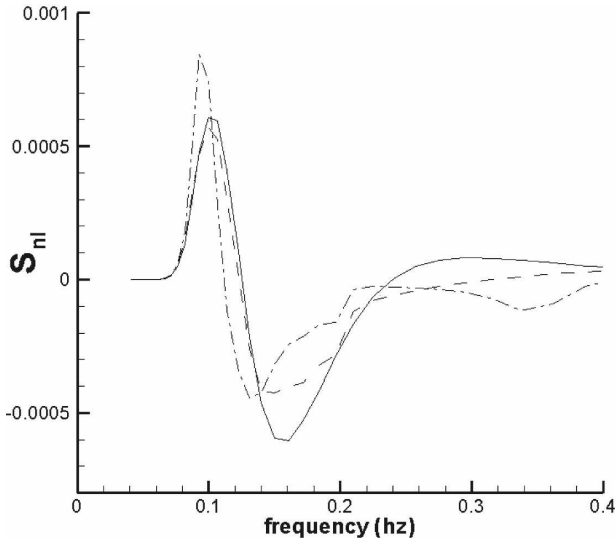


FIG. 5. Comparisons of the TSA results to the FBI solution for JONSWAP spectra with peakednesses equal to 1. Also shown is the contribution to the TSA from the parametric solution alone. (solid: full integral FBI, dash: TSA, dotted-dashed: parametric alone). The latter assumes an f^{-4} tail, whereas the test spectrum has an f^{-5} tail. Units are $m^2 Hz^{-1} s^{-1}$ for S_{ni} .

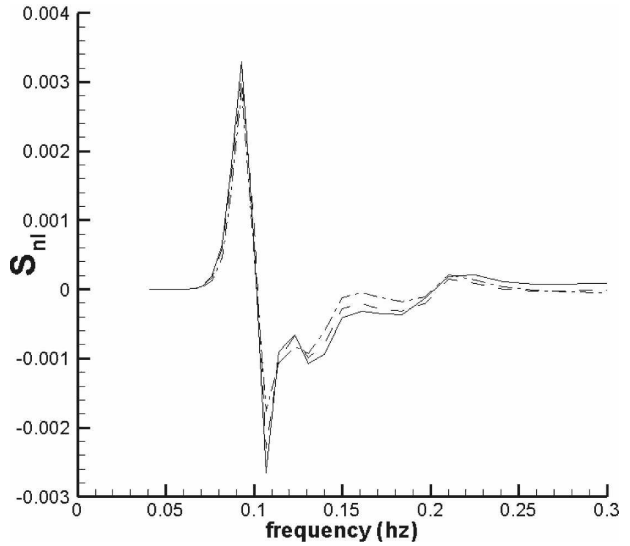


FIG. 6. As in Fig. 5, but with peakednesses equal to 3.3.

first approximation to the directionally integrated transfer rates for each spectrum. However, in each case, although the parametric representations also take into account variations in peakedness, the addition of the L -scale and X -scale terms into the TSA is seen to improve the agreement between the full-integral solution and the TSA approximation. Appendix B provides plots of energy transfer rates as a function of both frequency and direction for the full integral, the TSA, and the DIA, along with a discussion of how these compare to each other.

In the case of the Pierson–Moskowitz spectrum ($\gamma = 1$), the broadscale solution slightly misplaces the positive transfer lobe toward lower frequencies and overestimates its magnitude by about 50%. The use of additional terms in the TSA formulation moves the positive lobe into good agreement in terms of both location and magnitude. In both the negative lobe region and the high-frequency region, the addition of the TSA local-scale transfers help move the displaced midfrequency energy sink into closer agreement with the full-integral solution, but the improvement is not as marked as it is for the initial positive lobe.

In the case of the standard JONSWAP spectrum ($\gamma = 3.3$), the additional TSA terms reduce the undershoot of the parameterized solution, relative to the parametric solution alone, in the low-frequency positive lobe, by slightly over 20%, and in the midrange negative lobe, by slightly over 40%. In the high-fre-

quency region the additional TSA terms also reduce the deviations from the full-integral solution by over 50%. In the case of the very peaked spectrum ($\gamma = 7$), the additional TSA terms result in improvements over the parametric (B scale) solution by magnitudes that are similar to those of the standard JONSWAP spectrum ($\gamma = 3.3$). Moreover, we observe that the TSA errors in the nonlinear transfer become smaller with increasing peakedness.

Figures 5, 6, and 7 suggest that the TSA could have considerable promise for wave modeling since, unlike the DIA, it appears to capture the primary transfer patterns for a range of spectral peakedness values.

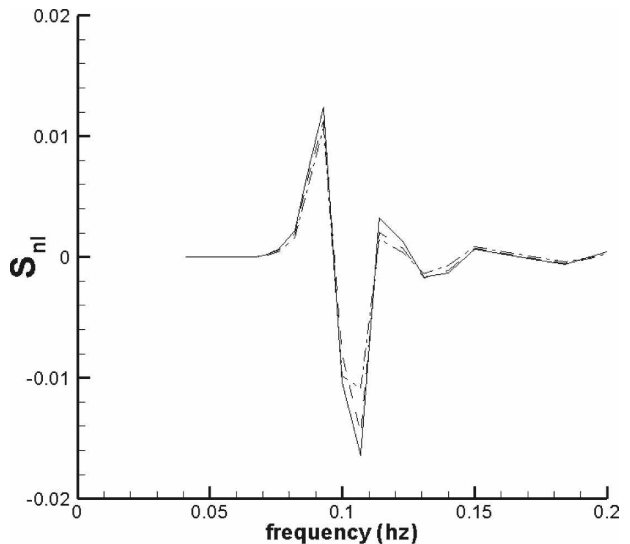


FIG. 7. As in Fig. 5, but with peakednesses equal to 7.

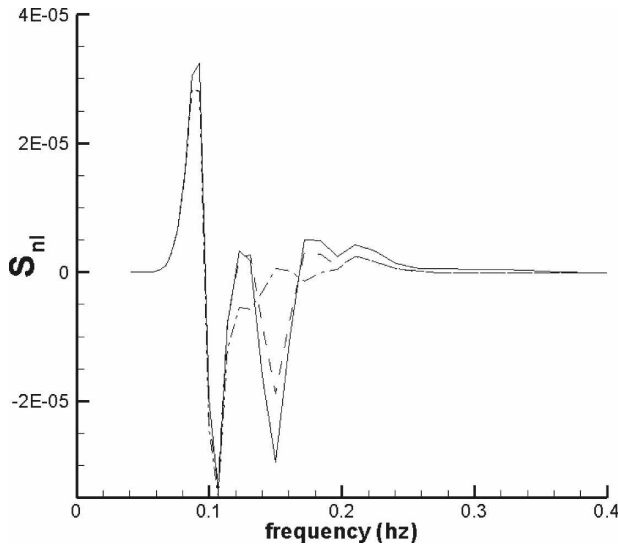


FIG. 8. Results for (i) complete integral solution, (ii) parametric-only interactions, and (iii) TSA for the case of $\kappa = 2.2$ and a $\cos^4\theta$ angular spreading with a secondary positive Gaussian perturbation superposed on the spectrum at $f/f_p = 1.5$; i.e., $A_z = 1$. Units are $\text{m}^2 \text{Hz}^{-1} \text{s}^{-1}$ for S_{nl} .

However, because the B -scale interactions represent a significant portion of the total interactions and appear to capture much of the basic shape of the overall transfer function, these cases may not provide a strong argument that this approximation will work well for spectral shapes with significant local deviations from a broad parametric shape. To investigate the suitability of the TSA for more complex spectra, we examine some results for spectra with perturbations added to them. Previous investigations (Perrie et al. 2004) have shown that the DIA does a poor job in representing the complex cases that we now examine.

Using a spectral shape similar to that of Resio and Perrie (1989), with an added Gaussian energy perturbation, yields an equation of the form

$$E(f, \theta) = \frac{\alpha u g f^{-4}}{(2\pi)^3} \Psi_1\left(\frac{f}{f_p}\right) \Psi_2(\theta - \theta_0) + Z(f - f_z, \theta - \theta_z), \quad (17)$$

where u as the wind speed and Ψ_1 is defined as

$$\Psi_1\left(\frac{f}{f_p}\right) = \kappa^{\exp(P)}.$$

Here, $P = (f - f_p)^2 / 2\sigma^2 f_p^2$ and $\sigma = 0.07$ for $f < f_p$, $= 0.09$, otherwise, and

$$\Psi_2(\theta - \theta_0) = \frac{\cos^m(\theta - \theta_0)}{\int_{-\pi/2}^{\pi/2} \cos^m(\theta - \theta_0) d\theta}.$$

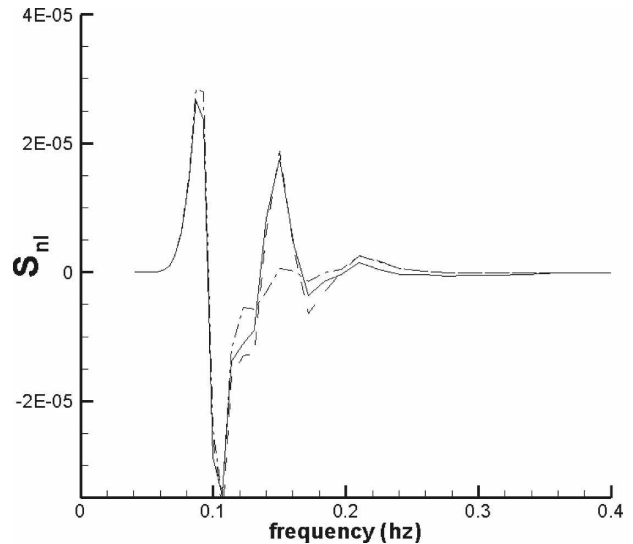


FIG. 9. As in Fig. 8, but for a negative Gaussian perturbation; i.e., $A_z = -1$. Units are $\text{m}^2 \text{Hz}^{-1} \text{s}^{-1}$ for S_{nl} .

For the tests shown here, $m = 4$, and the perturbation term is given in terms of a bivariate Gaussian form

$$Z(f - f_z, \theta - \theta_z) = A_z \exp\left(\frac{-\hat{\theta}^2}{2}\right) \exp\left(\frac{-\hat{f}^2}{2}\right), \quad (18)$$

where $\hat{\theta} = (\theta - \theta_z)/\sigma_\theta$ and $\hat{f} = (f - f_z)/\sigma_f$; parameter values are

$$f_z = 1.5f_p, \quad \theta_z = \theta_0, \quad \sigma_\theta = 0.3 \text{ rad}, \\ \sigma_f = 0.1 \text{ Hz}, \quad \text{and} \quad A_z = 1.0.$$

In this case, the parameterized spectral shape will be taken as the first term in Eq. (17), leaving the perturbation term exactly equal to the second term multiplied by the local energy density. Figure 8 gives the results for the complete integral solution, the parametric-only interactions, and the TSA for the case of $\kappa = 2.2$ (characteristic of a local sea spectrum) and a $\cos^4\theta$ angular spreading function. As the parameterization does not have any information on the perturbation, it retains precisely the same form as if the positive perturbation did not exist. The addition of the L -scale and X -scale interactions in the TSA does a good job in capturing the effects of the perturbation. In this case, the perturbation induces a second positive lobe into the nonlinear transfers. This serves to shift the peak forward on top of the equilibrium range at an accelerated pace compared to what might happen with no broadscale energy present.

Figure 9 provides results similar to those in Fig. 8, keeping all the same parameters as in the latter case except that we change the sign of the perturbation; that

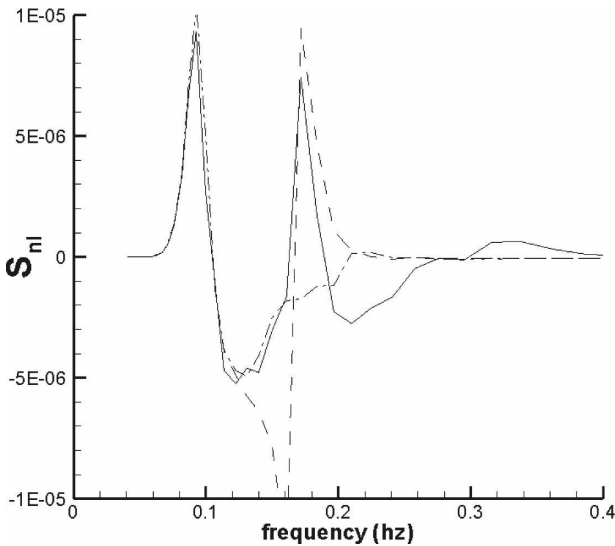


FIG. 10. Results for a case in which the spectrum contains a 40° discontinuity at $f = 1.5f_p$, retaining the same values for $E(f)$ as though the spectrum had not been shifted: Case with 40° angle shift at $1.5f_p$. Units are $\text{m}^2 \text{Hz}^{-1} \text{s}^{-1}$ for S_{nl} .

is, $A_z = -1$. Again, the L -scale and X -scale interactions do a good job in capturing the effects of the perturbations. In this case, the nonlinear transfers act to shift the negative perturbations into lower frequencies.

In tests shown in Figs. 8 and 9, the central angle of the perturbation is identical to the mean angle of the parametric spectrum. Figure 10 shows the results for a case in which the spectrum contains a 40° discontinuity at $f = 1.5f_p$, retaining the same values for $E(f)$ as though the spectrum had not been shifted. A $\cos^4\theta$ angular spreading function is used for this case and $\kappa = 1.2$. In this case, although the TSA captures the magnitudes of the positive lobes at both the spectral peak and the region immediately above the angular discontinuity along with the positions of these lobes, it overestimates the negative lobe by a factor of ~ 2 . While this performance is still markedly superior to the performance of the DIA for this type of case, we feel that it may be possible to improve upon these results by paying additional attention to the treatment of the B -scale interactions, which was intentionally kept quite simple in this paper.

As a final test of the TSA, we shall examine its performance for the same finite depth case shown previously for the DIA, using exactly the same combination of B -scale parameterization and L -scale and X -scale interactions as for the deep water cases. The only difference is that each of the B -scale, L -scale, and X -scale terms are computed using the actual depth of 10.5 m in the evaluation of the three matrices needed for the evaluation of Eq. (13) [$\mathbf{B}(f, \theta, \kappa)$, $\Lambda_p(f, \theta, \kappa)$, and $\Lambda_d(f,$

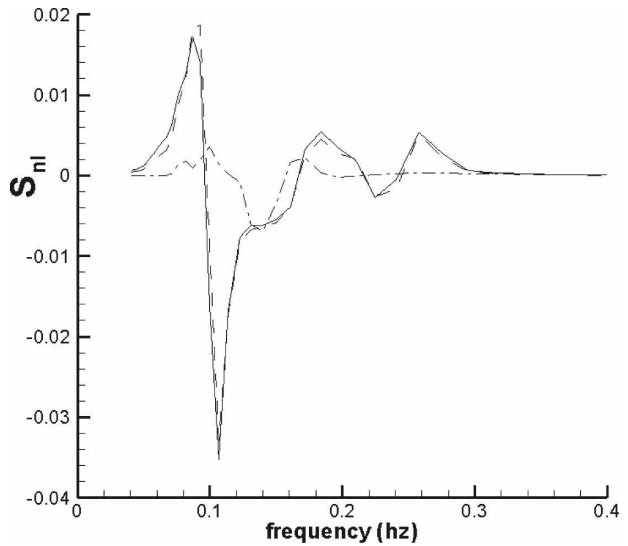


FIG. 11. Results for the full-integral solution, TSA, and the DIA, using the actual depth of 10.5 m. Finite-depth $kh = 0.7$ case, where solid line is full integral, dashed is TSA, and dotted-dashed is DIA. Units are $\text{m}^2 \text{Hz}^{-1} \text{s}^{-1}$ for S_{nl} .

θ, κ]. In general, for finite depth applications, a second free parameter ($k_p h$) could be used to represent the B -scale terms quite accurately, based on a suitable discretization. Figure 11 shows the results for the full-integral solution, TSA, and the scaled DIA. It is clear that the TSA has captured the finite depth effects quite well, and certainly much better than the application of the Herterich and Hasselmann (1980) similarity function to values beyond its region of applicability.

5. Discussion and conclusions

For wave models to accurately represent the detailed balance of the source terms responsible for wave generation and decay under a wide range of conditions, it is essential that each of the three primary terms contributing to this balance be realistically depicted for a substantial range of spectral shapes. For over 20 years, the only approximation for four-wave interactions that has shown utility for detailed-balance wave modeling has been the discrete interaction approximation, or DIA. This paper has demonstrated that significant problems exist with the DIA estimates of nonlinear transfers in deep water. These errors cannot be “tuned out” since the DIA is based on a reduced form of the Boltzmann integral that does not include the majority of the actual interactions within a spectrum. In shallow water the extrapolation of scaling arguments, owing to Herterich and Hasselmann (1980), into regions well beyond the appropriate range for this approximation renders estimates of nonlinear transfers in detailed-

balance models very inaccurate when applied in depths typical of coastal regions.

This paper introduces a new approximation, the two-scale approximation (TSA), based on the separation of a spectrum into a broadscale component and a local-scale (perturbation) component. This new method relies on a parametric representation of the broadscale spectral structure, while preserving the degrees of freedom essential to a detailed-balance source term formulation via the inclusion of the second scale in the approximation. This approximation appears to provide significantly increased accuracy over the DIA in all regions of the spectrum for all of the cases examined in this paper. Of particular importance is the very large improvement over the DIA for the finite depth case examined. It is important to note that this new approximation is based on the actual structure of the full-integral solution and uses no tuning coefficients to achieve the results.

Acknowledgments. The authors would like to acknowledge the valuable contributions of the anonymous reviewers to this paper. Their detailed reviews greatly improved both the content and accuracy of this manuscript. Support for this research comes from the U.S. Army Corps of Engineers MORPHOS program, the Canadian Panel on Energy Research and Development (PERD–Offshore Environmental Factors Program), ONR (U.S. Office of Naval Research) through the Gulf of Maine Ocean Observing System (GoMOOS), the Southeast University Research Association Coastal Ocean Observing and Prediction (SCOOP) program, and the Canada Foundation for Climate and Atmospheric Studies. The authors also wish to acknowledge the Office, Chief of Engineers, U.S. Army Corps of Engineers for permission to publish this paper.

APPENDIX A

A Sharp Perturbation Superposed on a Broad Equilibrium Range

The two-scale approximation offers some unique opportunities to examine the dynamics of spectral evolution for the case of two interacting wave trains or, as will be shown here, for the case of a perturbation superposed on a background spectrum. If a very sharp perturbation is located at wavenumber k , all of the integrals involving n'_2 and n'_4 not retained in Eq. (12) become vanishingly small.

Given a background spectrum, defined as

$$n(\mathbf{k}) \sim \beta k^{-4},$$

it is expected that the broadscale contributions to the total integral will be essentially zero (as this is a non-divergent flux form). Furthermore, if this broad scale is sufficiently large that the coupling coefficient becomes very small for interactions between waves in the center of this region and waves outside of this region, the rate of change of action for a perturbation in the center of such a region can be written as the second term in Eq. (11):

$$\frac{\partial n_1}{\partial t} = \iint \oint N_*^{\beta} C |\partial W / \partial n|^{-1} ds k_3 d\theta_3 dk_3 = (L + X)_*,$$

which shows that the interactions will be governed by local interactions L and cross-interactions ∂n involving the density terms

$$\begin{aligned} N_*^{\beta} &= \hat{n}_2 \hat{n}_4 (n'_3 - n'_1) + n'_1 n'_3 (\hat{n}_4 - \hat{n}_2) + \hat{n}_1 n'_3 (\hat{n}_4 - \hat{n}_2) \\ &+ n'_1 \hat{n}_3 (\hat{n}_4 - \hat{n}_2). \end{aligned}$$

Since the perturbation is very sharp, the product $n'_1 n'_3$ will be zero because only one of these two interacting wavenumbers will be nonzero for a very sharp perturbation. The transfer of action density from a region located in the vicinity of the perturbation can be written as

$$\frac{\delta n'}{\delta t} = n' \hat{n} \oint (\hat{n}_4 - \hat{n}_2) C \left| \frac{\partial W}{\partial n} \right|^{-1} ds k d\theta_3 dk.$$

After some algebra and assuming that contributions among the perturbed densities remain small, it can be shown that the perturbation will decay according to an equation of the form:

$$\frac{\partial n'}{\partial t} \sim \beta^2 n'.$$

Thus, although the fundamental cubic relationship for the nonlinear transfers is preserved, the two-scale approximation shows that the dominant contributions in this case will come from a quadratic dependence on the equilibrium range coefficient and only a linear dependence on the perturbation magnitude itself. Although this may be an oversimplification for many practical cases, it should provide a first-order approximation to the magnitude of the relaxation times expected for a return to equilibrium values, given a perturbation imbedded within an equilibrium range.

APPENDIX B

Two-Dimensional Transfer Rates from the Full Integral, TSA, and DIA

Figure B1 shows contours of $S_{nl}(f, \theta)$ full Boltzmann integral (FB10), the TSA, and the DIA, respectively, for

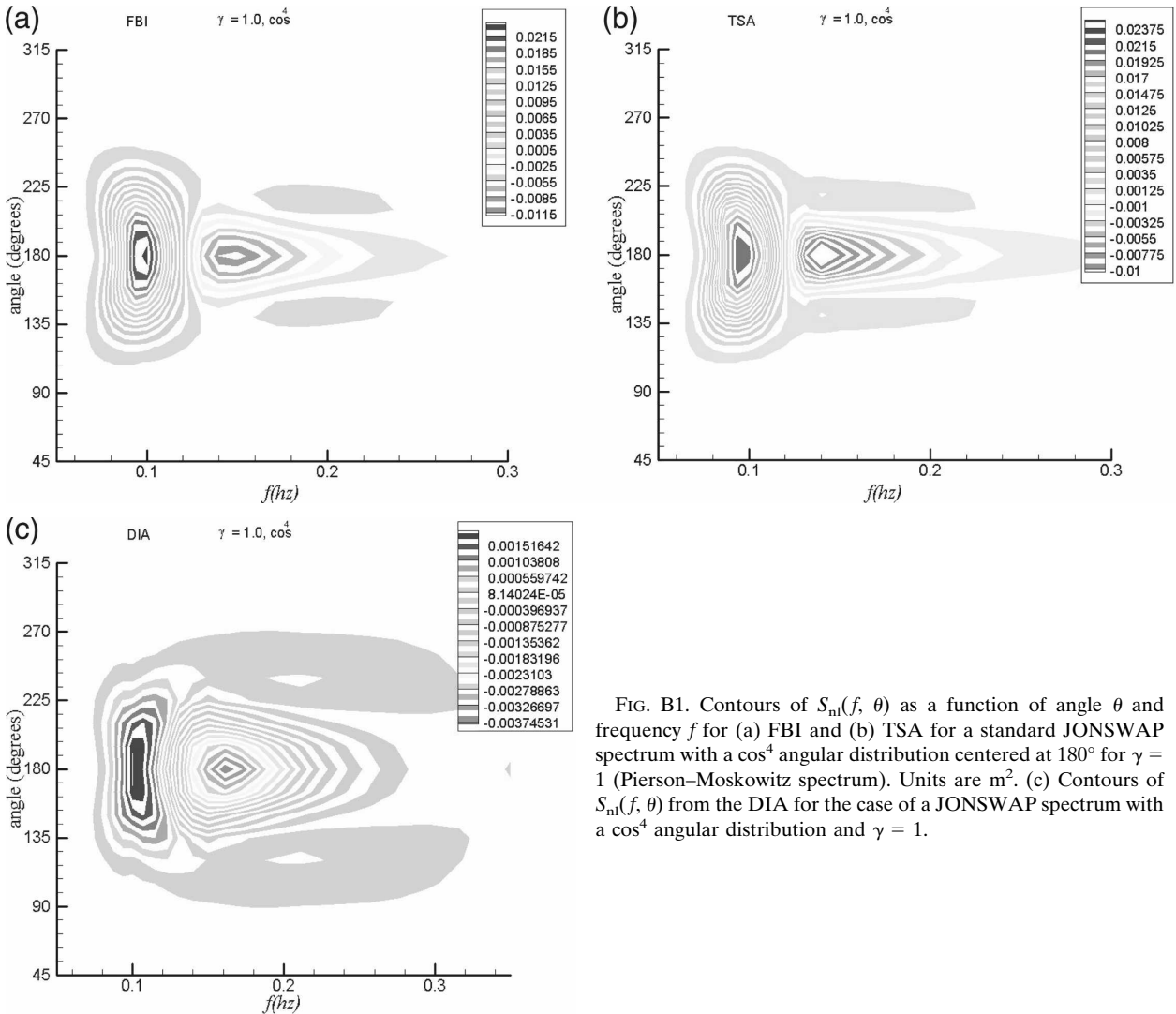


FIG. B1. Contours of $S_{ni}(f, \theta)$ as a function of angle θ and frequency f for (a) FBI and (b) TSA for a standard JONSWAP spectrum with a \cos^4 angular distribution centered at 180° for $\gamma = 1$ (Pierson–Moskowitz spectrum). Units are m^2 . (c) Contours of $S_{ni}(f, \theta)$ from the case of a JONSWAP spectrum with a \cos^4 angular distribution and $\gamma = 1$.

the case of a JONSWAP spectrum with a \cos^4 angular distribution centered at 180° for the case of $\gamma = 1$ (Pierson–Moskowitz spectrum). These comparisons correspond to the directionally integrated comparisons shown in Fig. 2 for the DIA and Fig. 5 for the TSA. All three of the directional patterns are in rough qualitative agreement with a broad positive peak located in the region from 0.07 to 1.1 Hz, a negative lobe in the angles near the mean angle centered on frequencies from 0.14 to 0.18 Hz, and positive lobes to either side of the negative lobes in this same frequency range. These results capture the tendency for nonlinear energy transfers to broaden the spectrum for frequencies less than the spectral peak and to tend toward a bimodal form at high frequencies as seen in many observations (Long and Resio 2007).

An interesting aspect of the comparison between the

FBI solution and the TSA can be seen in frequencies above ~ 0.28 Hz. In this area, the differences between the f^{-5} -based JONSWAP spectrum and the f^{-4} -based parametric basis (as used here) cannot be totally compensated by the local-scale terms included in the TSA. However, the overall transfer rates are relatively small here, so this is arguably not too important for applications to wave modeling.

Figure B2 shows contours of $S_{ni}(f, \theta)$ from the full integral, the TSA, and the DIA, respectively, for the case of a JONSWAP spectrum with a \cos^4 angular distribution centered at 180° for the case of $\gamma = 3.3$ (standard JONSWAP spectrum). These comparisons correspond to the directionally integrated transfers shown in Fig. 1 for the DIA and Fig. 6 for the TSA. In this case, the degree of agreement between the TSA and FBI is excellent throughout the entire range of the compari-

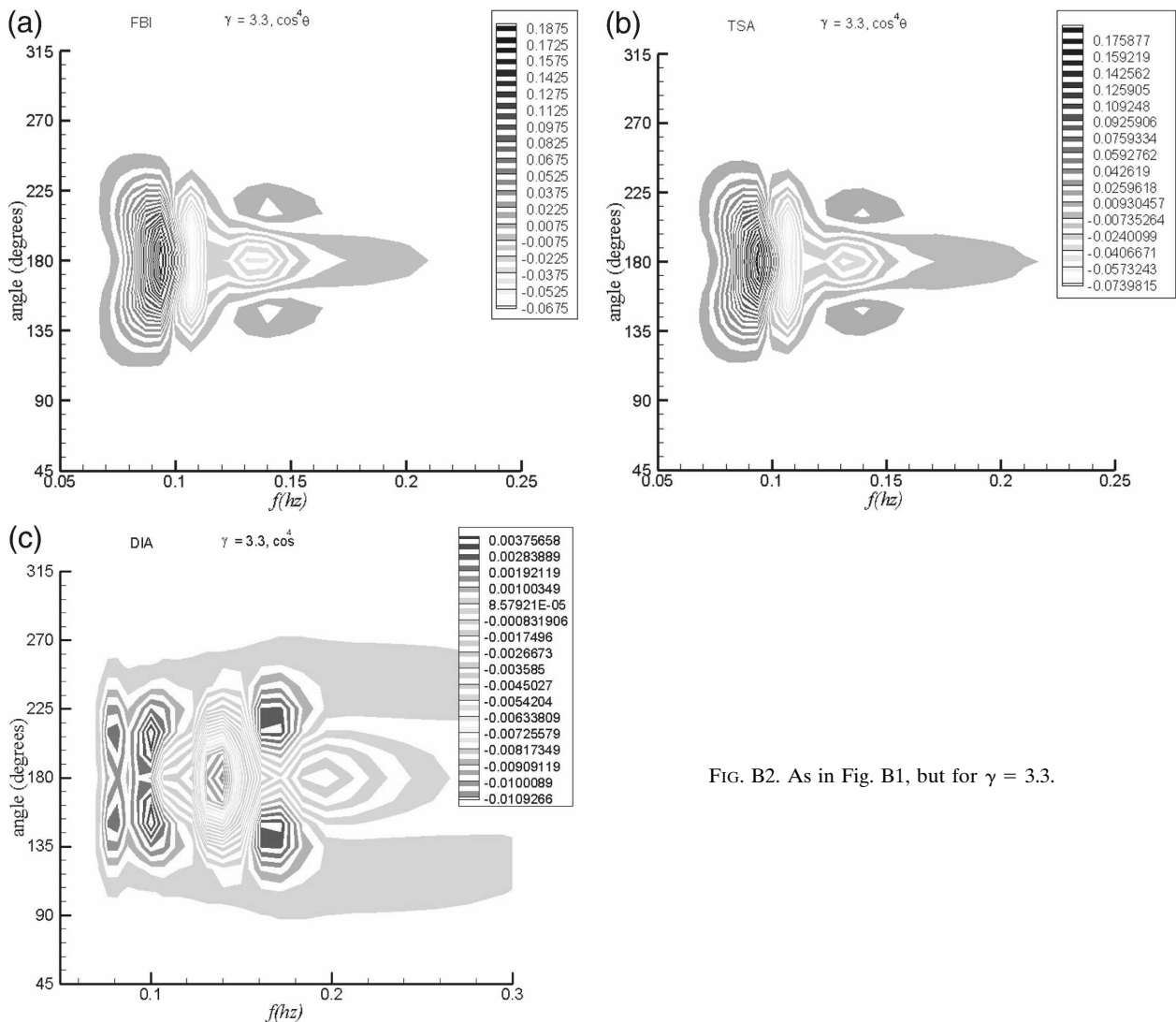


FIG. B2. As in Fig. B1, but for $\gamma = 3.3$.

son. The DIA appears to essentially miss the dominant negative lobe found in the range of 0.1 to 0.12 Hz in both FBI and TSA results. The DIA does exhibit a dominant negative lobe in the 0.12 to 0.14 Hz range, where both the FBI and TSA results exhibit secondary negative lobes. These differences in the directional distributions of the TSA and the DIA clearly will have a pronounced difference on the modeled distributions of wave angles in a spectrum.

Figure B3 shows contours of $S_{ni}(f, \theta)$ from the FBI, TSA, and DIA results, respectively, for the case of a JONSWAP spectrum with a \cos^4 angular distribution centered at 180° for the case of $\gamma = 7$ (JONSWAP spectrum). These comparisons correspond to the directionally integrated transfers shown in Fig. 3 for the DIA and Fig. 7 for the TSA. As was seen for this JONSWAP spectrum, the degree of agreement between the TSA

and FBI results is good throughout the entire range of the comparison. The DIA again misses the dominant negative lobe of the interactions in the region 0.1 to 0.12 Hz but exhibits a dominant negative lobe at the location where both the FBI and TSA results show a relatively minor secondary minimum in their transfers. Another difference can be seen at still higher frequencies (0.15 to 0.2 Hz) where the DIA exhibits a strong positive lobe near the mean spectral angle, whereas both FBI and TSA results do not suggest the presence of a strong positive source in this range of frequencies and angles.

It is encouraging that the TSA appears to provide a very reasonable representation to $S_{ni}(f, \theta)$ for all of these cases and qualitatively captures all of the essential features of these transfers. Such faithful representation of the directional characteristics of $S_{ni}(f, \theta)$ can play an

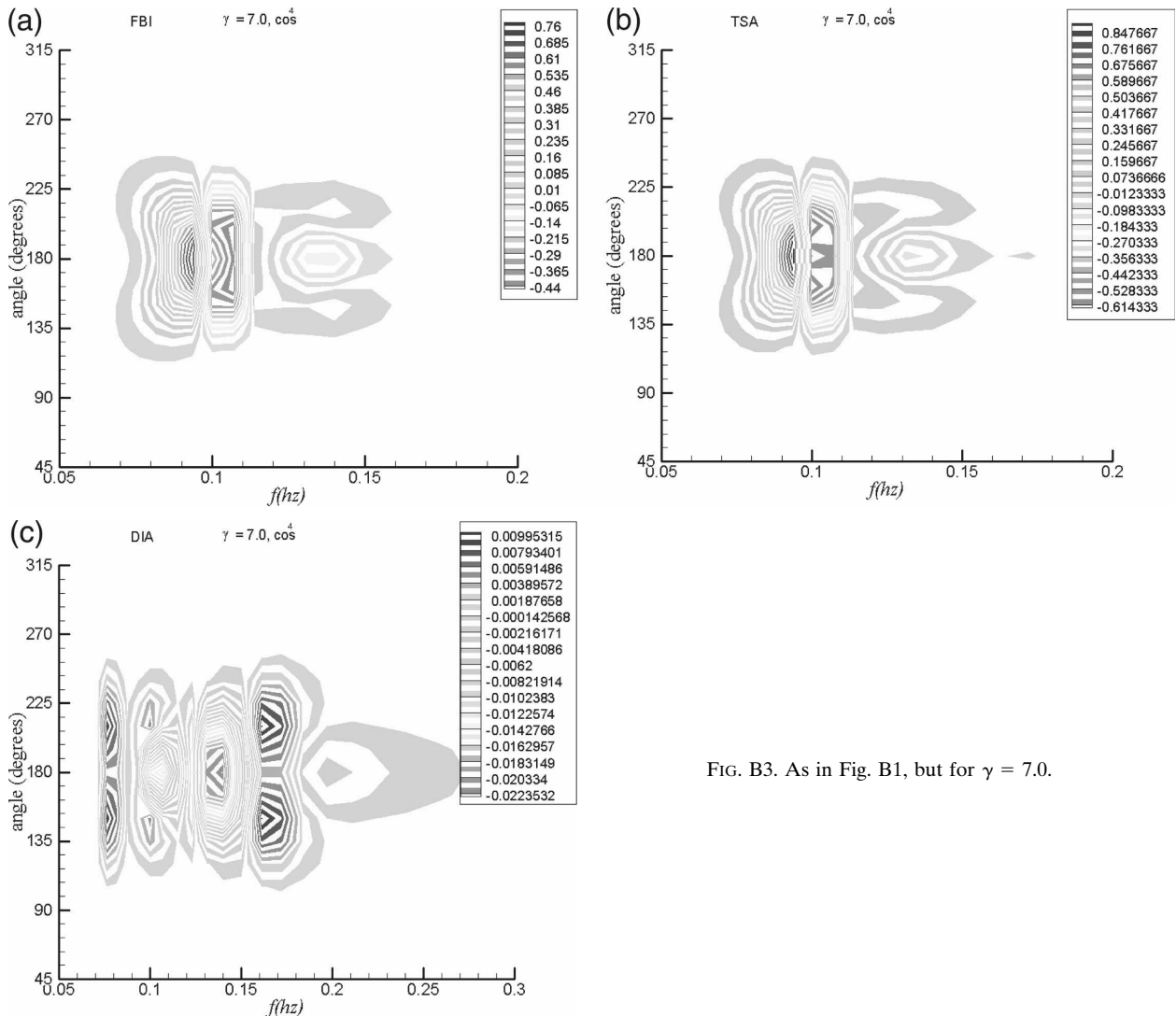


FIG. B3. As in Fig. B1, but for $\gamma = 7.0$.

important role in improving near-coast, slanting fetch, and narrow fetch model applications. The DIA roughly captures some of the same features but misses potentially important parts of the overall transfers at frequencies just above the spectral peak.

REFERENCES

Barnett, T. P., 1968: On the generation dissipation and prediction of ocean wind waves. *J. Geophys. Res.*, **73**, 513–530.

Benoit, M., 2005: Evaluation of methods to compute the nonlinear quadruplets interactions for deep-water spectra. *Proc. Fifth Int. Symp. on Ocean Waves Measurement and Analysis*, Madrid, Spain, ASCE 52, 1–10.

Booij, N., R. C. Ris, and L. H. Holthuijsen, 1999: A third-generation wave model for coastal regions 1. Model description and validation. *J. Geophys. Res.*, **104**, 7649–7666.

Bouws, E., H. Günther, W. Rosenthal, and C. L. Vincent, 1985:

Similarity of the wind wave spectrum in finite depth water 1. Spectral form. *J. Geophys. Res.*, **90**, 975–986.

Donelan, M. A., 1980: Similarity theory applied to the forecasting of wave heights, periods, and directions. *Proc. Canadian Coastal Conf.*, Burlington, Ontario, Canada, National Research Council, 47–61.

—, J. Hamilton, and W. H. Hui, 1985: Directional spectra of wind-generated waves. *Philos. Trans. Roy. Soc. London*, **A315**, 509–562.

Ewing, J. A., 1971: A numerical wave prediction method for the North Atlantic Ocean. *Dtsch. Hydrogr. Z.*, **24**, 241–261.

Hasselmann, K., 1962: On the nonlinear energy transfer in a gravity wave spectrum. Part 1. *J. Fluid Mech.*, **12**, 481–500.

—, and Coauthors, 1973: *Measurements of Wind-Wave Growth and Swell Decay during the Joint North Sea Wave Project (JONSWAP)*. *Ergänzungsheft zur Deutschen Hydrographischen Zeits.*, 95 pp.

Hasselmann, S., and K. Hasselmann, 1985: Computations and parameterizations of the nonlinear energy transfer in a gravity wave spectrum. Part I: A new method for efficient computa-

- tions of the exact nonlinear transfer integral. *J. Phys. Oceanogr.*, **15**, 1369–1377.
- , —, J. H. Allender, and T. P. Barnett, 1985: Computations and parameterizations of the nonlinear energy transfer in a gravity-wave spectrum. Part II: Parameterizations of the nonlinear energy transfer for application in wave models. *J. Phys. Oceanogr.*, **15**, 1378–1391.
- Herterich, K., and K. Hasselmann, 1980: A similarity relation for the nonlinear energy transfer in a finite-depth gravity-wave spectrum. *J. Fluid Mech.*, **97**, 215–224.
- Komen, G. J., K. Hasselmann, and S. Hasselmann, 1984: On the existence of a fully developed windsea spectrum. *J. Phys. Oceanogr.*, **14**, 1271–1285.
- , L. Cavaleri, and M. Donelan, K. Hasselmann, S. Hasselmann, and P.A.E.M. Janssen, 1994: *Dynamics and Modelling of Ocean Waves*. Cambridge University Press, 532 pp.
- Lin, R. Q., and W. Perrie, 1997: A new coastal wave model. Part III: Nonlinear wave–wave interaction. *J. Phys. Oceanogr.*, **27**, 1813–1826.
- , and —, 1999: Wave-wave interactions in finite depth water. *J. Geophys. Res.*, **104**, 11 193–11 213.
- Long, C. E., and D. T. Resio, 2007: Wind wave spectral observations in Currituck Sound, North Carolina. *J. Geophys. Res.*, **112**, C05001, doi:10.1029/2006JC003835.
- Perrie, W., D. Resio, and A. Susilo, 2004: Energy-flux balances and source term parameterizations. *Proc. Eighth Int. Workshop on Wave Hindcasting and Forecasting*, Oahu, HI, 10 pp. [Available online at <http://www.waveworkshop.org/8thWaves/Papers/Q3.pdf>.]
- Petterson, H., 2004: Wave growth in a narrow bay. Ph.D. dissertation, University of Helsinki, 33 pp.
- Phillips, O. M., 1960: The dynamics of unsteady gravity waves of finite amplitude. *J. Fluid Mech.*, **9**, 193–217.
- Polnikov, V. G., 2002: A basing of the diffusion approximation derivation for the four-wave kinetic integral and properties of the approximation. *Nonlinear Processes Geophys.*, **9**, 355–366.
- Pushkarev, A. N., D. Resio, and V. E. Zakharov, 2004: Second generation diffusion model of interacting gravity waves on the surface of deep fluid. *Nonlinear Processes Geophys.*, **11**, 329–342.
- Resio, D. T., 1981: The estimation of wind-wave generation in a discrete spectral model. *J. Phys. Oceanogr.*, **11**, 510–525.
- , and W. Perrie, 1989: Implications of an f^{-4} equilibrium range for wind-generated waves. *J. Phys. Oceanogr.*, **19**, 193–204.
- , and —, 1991: A numerical study of nonlinear energy fluxes due to wave-wave interactions. Part 1: Methodology and basic results. *J. Fluid Mech.*, **223**, 609–629.
- , J. H. Pihl, B. A. Tracy, and C. L. Vincent, 2001: Nonlinear energy fluxes and the finite depth equilibrium range in wave spectra. *J. Geophys. Res.*, **106**, 6985–7000.
- Tracy, B. A., and D. T. Resio, 1982: Theory and calculation of the nonlinear energy transfer between sea waves in deep water. U.S. Army Engineer Waterways Experiment Station WES Rep. 11, 52 pp.
- Van Vledder, G. Ph., 2006: The WRT method for the computation of non-linear four-wave interactions in discrete spectral wave models. *Coastal Eng.*, **53**, 223–242.
- WAMDI Group, 1988: The WAM model—A third generation oceans wave prediction model. *J. Phys. Oceanogr.*, **18**, 1775–1810.
- Webb, D. J., 1978: Non-linear transfers between sea waves. *Deep-Sea Res.*, **25**, 279–298.
- Young, I. R., and G. Van Vledder, 1993: A review of the central role of nonlinear interactions in wind-wave evolution. *Philos. Trans. Roy. Soc. London*, **A342**, 505–524.
- Zakharov, V. E., and N. N. Filonenko, 1966: The energy spectrum for stochastic oscillation of a fluid's surface. *Dokl. Akad. Nauk SSSR*, **170**, 1992–1995.